Available online at www.sciencedirect.com

SciVerse ScienceDirect

Ceramics International 38 (2012) 5095–5102

CERAMICS INTERNATIONAL

www.elsevier.com/locate/ceramint

Structural, thermal and electrical studies of a novel rubidium phosphite tellurate compound

Berceste Beyribey [a,b,*], Jonathan Hallinder [a]

[a] Fuel Cells and Solid State Chemistry Division, Risø National Laboratory, Technical University of Denmark, DK-4000 Roskilde, Denmark

[b] Chemical Engineering Department, Faculty of Chemical and Metallurgical Engineering, Yildiz Technical University, TR-34210 Istanbul, Turkey

Received 2 February 2012; received in revised form 3 March 2012; accepted 4 March 2012

Available online 12 March 2012

Abstract

Structural, thermal and electrical properties studies of rubidium phosphite tellurate, $RbH(PO_3H)\cdot Te(OH)_6$, were performed. An endothermic peak, which reached a completion at about 315 °C accompanied with a weight loss of 4.6 wt.%, was attributed to dehydration. Four types of pellets were produced, namely pellets A, B, C and D. Pellet A was tested with platinum–carbon paper electrode, and pellets B, C and D were tested with gold electrodes. Both pellets A and B were studied from 113 °C to 317 °C for 135 h. Pellet C was first investigated from room temperature to 176 °C for 360 h. After cooling down to room temperature, a second measurement with pellet C was carried out under the same conditions as used for pellets A and B. Pellet D, on the other hand, was heated up to 450 °C, kept at that temperature for 2 h and then cooled down to room temperature prior to the conductivity measurements. It was observed that the conductivities of pellets A and B decreased to values of 5.2×10^{-8} S cm^{-1} and 6.6×10^{-7} S cm^{-1} at 317 °C, respectively, and an unexpected rise in the conductivity (9.89×10^{-6} S cm^{-1} at 317 °C) was seen with pellet C. Dehydration of $RbH(PO_3H)\cdot Te(OH)_6$ might be responsible for this unexpected rise in the conductivity of pellet C. The monoprotic part $RbH(PO_3H)$ of $RbH(PO_3H)\cdot Te(OH)_6$ apparently became diprotic ($Rb_2H_2P_2O_5$) part of $Rb_2H_2P_2O_5\cdot[Te(OH)_6]_2$ after dehydration. The measured conductivity of pellet D, which was dehydrated prior to the measurement, reached a value of 5.41×10^{-5} S cm^{-1} at 317 °C and showed a good stability over-each-run time and temperatures measurement up to 317 °C. The dehydrated compound, $Rb_2H_2P_2O_5\cdot[Te(OH)_6]_2$, has also a higher hydrogen density relative to the starting compound, $RbH(PO_3H)\cdot Te(OH)_6$. It is deduced that completion of the dehydration can be responsible for the unexpected rise in the conductivity of $RbH(PO_3H)\cdot Te(OH)_6$. This unusual case is important for studies in solid acid proton conductors.

Keywords: Solid acids; Rubidium dihydrogen phosphite tellurate; Proton conductivity; Impedance spectroscopy; Thermal analysis

1. Introduction

Many acid salts of inorganic oxy-acids have gained attention as promising electrolytes. Some of their properties, such as proton conductivity or ferroelectric transition, are due to specific features of hydrogen bonds formed in crystal structures of these compounds [1–3].

Alkali-metal acid sulfates and acid phosphates have been studied in detail since Baranov and co-workers [4–6] demonstrated that the conductivity of $CsHSO_4$ increases with 2–3 orders of magnitude upon heating the material above its phase transition temperature where it goes from a monoclinic phase to a high-temperature tetragonal phase. On the other hand, the first systematic results on the crystal structures of acid phosphites, such as MH_2PO_3 (where $M = Rb^+$, Cs^+, Tl^+), $(MH_2PO_3H)_2\cdot H_3PO_3$ (where $M = Rb^+$, Tl^+) and $MH_2PO_3\cdot H_3PO_3$ (where $M = K^+$, Cs^+) were presented by Kosterina and co-workers [2,3]. Chisholm et al. [7] showed that cesium dihydrogen phosphite, $CsH(PO_3H)$, undergoes a transition, with an onset of 137 °C, to a phase with high proton conductivity. Zhou et al. [8] studied electrical conductivity of solid acid phosphites $MH(PO_3H)$ with $M = Li^+$, Na^+, K^+, Rb^+, Cs^+, NH_4^+ for the first time. They observed superprotonic conductivity following a phase transition in the temperature range from 120 to 190 °C for the monoclinic forms, including Na^+, K^+, Rb^+, Cs^+, NH_4^+

* Corresponding author at: Chemical Engineering Department, Faculty of Chemical and Metallurgical Engineering, Yildiz Technical University, TR-34210 Istanbul, Turkey.

E-mail address: berceste@yildiz.edu.tr (B. Beyribey).

0272-8842/$36.00
doi:10.1016/j.ceramint.2012.03.012

derivatives. No superprotonic phase transition was observed for orthorhombic $LiH(PO_3H)$. The conductivities of $KH(PO_3H)$ and $LiH(PO_3H)$ reached the values of $4.2 \times 10^{-3}\ \Omega^{-1}\ cm^{-1}$ (at 140 °C) and $3 \times 10^{-3}\ \Omega^{-1}\ cm^{-1}$ (at 160 °C), respectively. Bondarenko et al. [5] investigated a novel superprotonic $KH(PO_3H)$–SiO_2 composite electrolyte and showed that dispersion with nano-sized SiO_2 particles leads to improved mechanical properties.

Compounds with general formulas of $M_xM'_{(1-x)}AO_4{\cdot}Te(OH)_6$ and $M_2(AO_4)_x(A'O_4)_{(1-x)}{\cdot}Te(OH)_6$ (where M, M′ is Na^+, K^+, Rb^+, NH_4^+, Tl^+ and A, A′ = S^{2-}, Se^{2-}) were studied by Dammak and co-workers [9–25] and they showed that all of these compounds exhibit a superprotonic behavior. A proton conductivity of 8×10^{-2} S cm^{-1} in air at 357 °C was achieved for $Rb_2(SO_4)_{0.5}(SeO_4)_{0.5}{\cdot}Te(OH)_6$ [18]. The stability of phosphites in hydrogen atmosphere and the relatively high operating temperature of tellurate compounds inspired us to investigate rubidium phosphite tellurate, $RbH(PO_3H)Te(OH)_6$. This paper presents the first results of synthesis, structural, thermal and electrical studies on $RbH(PO_3H){\cdot}Te(OH)_6$.

2. Experimental

Rubidium carbonate (99.8%, Sigma–Aldrich), phosphorous acid (99%, Sigma–Aldrich) and telluric acid (99%, Sigma–Aldrich) with a molar ratio of 1:2:2 were dissolved in deionized water, separately. Concentrations of Rb_2CO_3, $H_2(PO_3H)$ and $Te(OH)_6$ solutions were 12.63 mmol/40 mL, 25.25 mmol/15 mL and 25.25 mmol/25 mL, respectively. The phosphorous acid solution was slowly added to the rubidium carbonate solution. After 1 h, telluric acid solution was added to the obtained solution. $RbH(PO_3H){\cdot}Te(OH)_6$ powder was obtained by slow evaporation of the aqueous solution continuously at approximately 50 °C during 2 days.

The reaction is:

$$Rb_2CO_3 + 2H_2(PO_3H) + 2Te(OH)_6 \rightarrow 2RbH(PO_3H)\cdot Te(OH)_6 + CO_2 + H_2O \quad \text{(R1)}$$

The powder was dried in an oven in air at about 130 °C during two weeks prior to experiments.

Scanning electron microscopy (SEM) and energy dispersive X-ray spectroscopy (EDS) analysis were carried out using a Zeiss Evo 60. EDS data were analyzed using the NSS 2.2 X-ray MicroAnalysis program. X-ray diffraction (XRD) data were recorded at room temperature using Stoe Theta-Theta XRD (40 kV, 30 mA, Cu $K\alpha_1$) and analyzed using the STOE Win XPOW 2.20 program. Thermogravimetry (TG) and differential thermal analysis (DTA) were carried out in air using TG–DTA system (Netzsch STA 409 CD) with a scan rate of 5 °C min^{-1}. Differential scanning calorimetry (DSC) experiments were performed in air by Netzsch DSC 200 F3, heating $RbH(PO_3H){\cdot}Te(OH)_6$ from room temperature to 500 °C with a scan rate of 5 °C min^{-1}. Samples were ground with an agate mortar prior the measurements.

Conductivity measurements were carried out using electrochemical impedance spectroscopy (EIS). Four pellets, namely pellet A, B, C and D were produced by pressing $RbH(PO_3H){\cdot}Te(OH)_6$ powders into discs of about 1 mm thickness and 8 mm diameter at 200 MPa pressure. The pellet A was tested with platinum–carbon paper electrode, and the pellets B, C and D were tested with gold electrodes. Gold electrodes were sputtered on both sides of the pellets B, C and D. Both the pellets A and B were investigated from 113 °C to 317 °C for 135 h. The pellet C was first investigated from room temperature to 176 °C for 360 h. After cooling down to room temperature, a second measurement with pellet C was carried out under the same conditions as used for the pellets A and B. The pellet D, on the other hand, was heated up to 450 °C, kept at that temperature for 2 h and then cooled down to room temperature at heating/cooling scan rate of 1 °C min^{-1} prior to the conductivity measurements. The heating procedures applied to the pellets are given schematically in Fig. 1.

The measurements were done under dry air ($pH_2O < 0.001$ bar), humidified air ($pH_2O = 0.1$ bar) and humidified gas mixture of 9% H_2 in N_2 ($pH_2O = 0.1$ bar). The gases were humidified by bubbling the gas through a heated water bottle ($T(H_2O) = 46$ °C). Impedance spectra were recorded under flowing gases (50 mL/min) using a Solartron 1260 frequency analyzer in all measurement series. An excitation voltage with amplitude of 20 mV was used. No bias voltage was

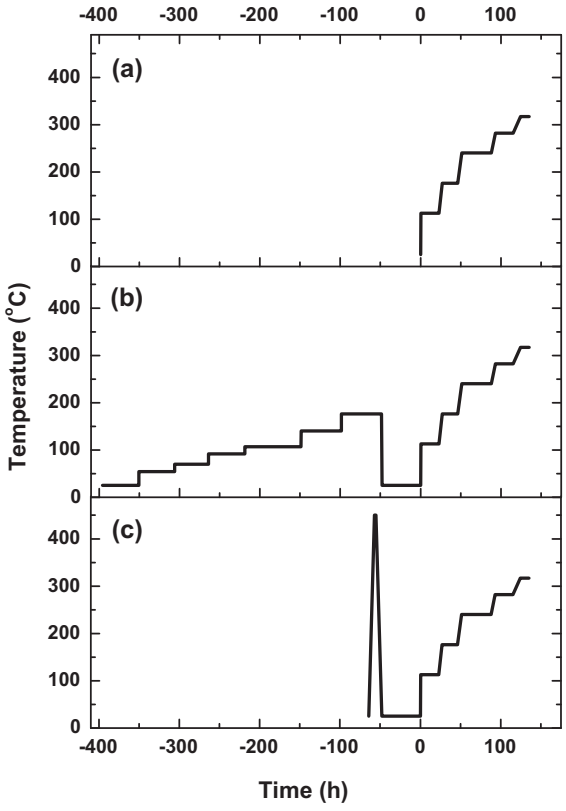

Fig. 1. The heating procedures applied to (a) the pellets A and B, (b) the pellet C and (c) the pellet D. The pellets A and B were tested for 135 h between 113 and 317 °C. The pellet C (earlier investigated at various temperatures up to 176 °C for 360 h) and the pellet D (heated up to 450 °C and then cooled down to room temperature prior to the measurement) were tested under the same conditions as used for the pellets A and B.

applied. The temperature of measurement was increased stepwise with heating rates of 5 °C min^{-1}. Measurements were carried out over the frequency range of 1 MHz to 1 Hz. Data analysis was done using the ZSimpWin 3.21 program.

3. Results

3.1. Structural and thermal analysis

Synthesis with slow evaporation resulted in $RbH(PO_3H)\cdot Te(OH)_6$ particles with diameters in the range of less than 1–60 μm. A SEM micrograph of the synthesized powder is shown in Fig. 2. It can be seen that smaller particles tend to form agglomerates. Fig. 3 shows the results of 5 EDS point analyses on the surface of the powder, which shows distribution of elements for different points.

Thermal analysis reveals the thermal behavior of the $RbH(PO_3H)\cdot Te(OH)_6$ powder and to monitor weight losses due to dehydration. Figs. 4 and 5a, respectively, indicate that both

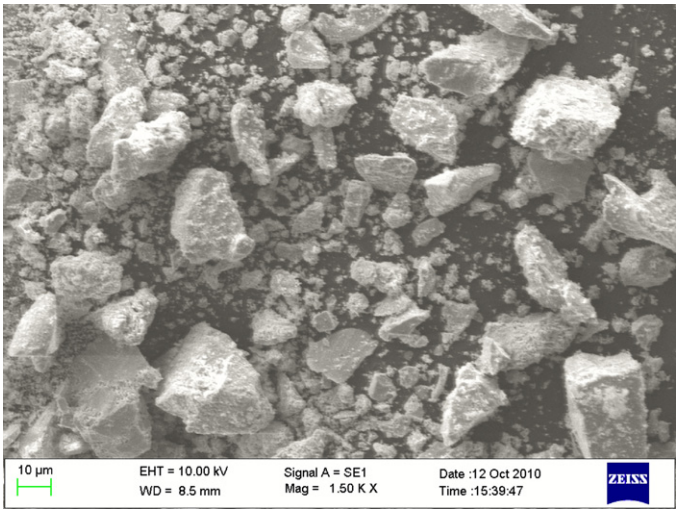

Fig. 2. SEM image taken from $RbH(PO_3H)\cdot Te(OH)_6$ powder which was synthesized by slow evaporation of the aqueous solution, 1500×.

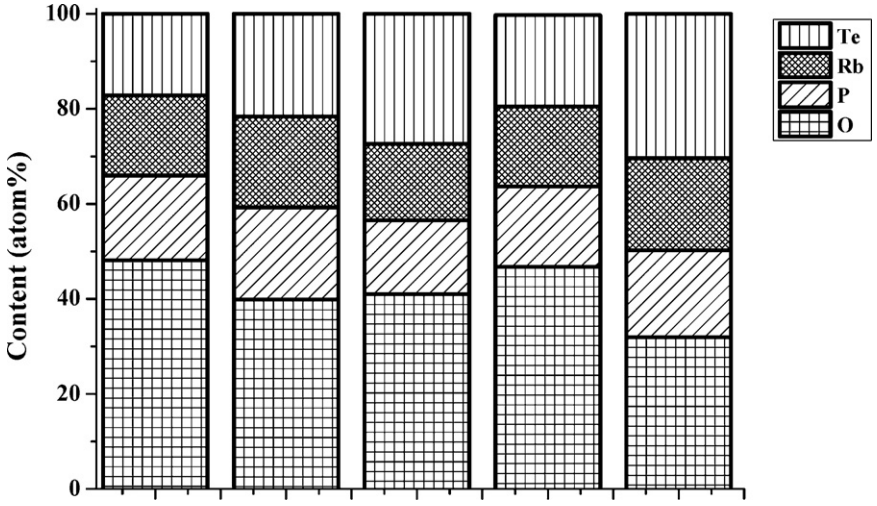

Fig. 3. Point analysis showing distribution of detectable elements at five different points on the surface of the synthesized $RbH(PO_3H)\cdot Te(OH)_6$ (hydrogen is not detectable by EDS analysis).

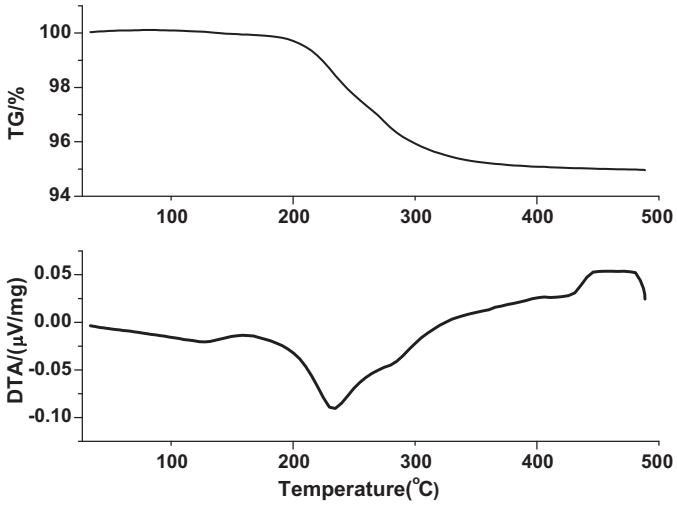

Fig. 4. TG/DTA analysis of the synthesized $RbH(PO_3H)\cdot Te(OH)_6$ at a scan rate of 5 K min^{-1}.

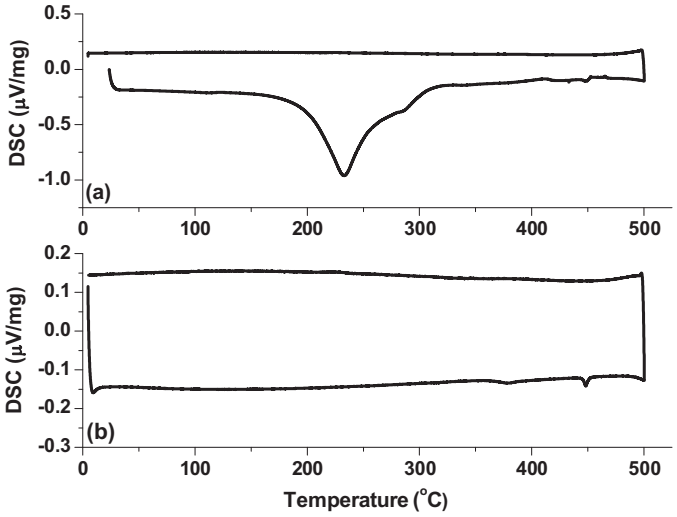

Fig. 5. DSC analysis of the synthesized $RbH(PO_3H)\cdot Te(OH)_6$ at a scan rate of 5 K min^{-1}: (a) first heating/cooling cycle and (b) second heating/cooling cycle.

DTA and DSC profiles of $RbH(PO_3H)\cdot Te(OH)_6$ show a pronounced endothermic peak at 233 °C on the first heating cycle. While cooling from a maximum temperature of 500 °C, no reverse of the first transition is seen in Fig. 5a. Moreover, Fig. 5b demonstrates neither an endothermic nor an exothermic peak occurs during the second heating/cooling cycles. The weight loss accompanied by the endothermic peak is completed at about 315 °C with a total loss of 4.6 wt.%. The weight loss is in a good agreement with the following dimerization reaction as given the same reaction for all $MH(PO_3H)$ compounds [5]:

$$2RbH(PO_3H)\cdot Te(OH)_6 \rightarrow Rb_2H_2P_2O_5\cdot[Te(OH)_6]_2 + H_2O \qquad \Delta H > 0 \qquad (R2)$$

Fig. 6a gives room temperature XRD patterns of the synthesized $RbH(PO_3H)\cdot Te(OH)_6$ indexing of amorphous and crystalline structures. Fig. 6b–e shows room temperature XRD patterns of the pellets A, B, C, D after the conductivity measurements. Fig. 6b and c represents a transformation from amorphous towards a more crystalline structure becomes visible for the tested pellets A and B, while it reaches the completion for the tested pellet C as seen in Fig. 6d. Fig. 6e illustrates the tested pellet D mainly has a crystalline structure with some residuals amorphous structure, it is seen that a complete dehydration of $RbH(PO_3H)\cdot Te(OH)_6$ was not achieved for a 2-h pretreatment at 450 °C.

3.2. Electrochemical impedance spectroscopy

Impedance spectra were obtained in the temperature range of 113–317 °C. Comparisons of conductivity results for the pellets A and B and for the pellets C and D are given in Figs. 7 and 8, respectively. As seen in Fig. 7, the measured conductivities of both pellets A and B increases by changing the atmosphere from dry air ($pH_2O < 0.001$ bar) to humidified air ($pH_2O = 0.1$ bar) at 113 °C. It increases further when changing the gas from humidified air to humidified gas mixture of 9%H_2 in N_2 ($pH_2O = 0.1$ bar) at 176 °C. The pellets

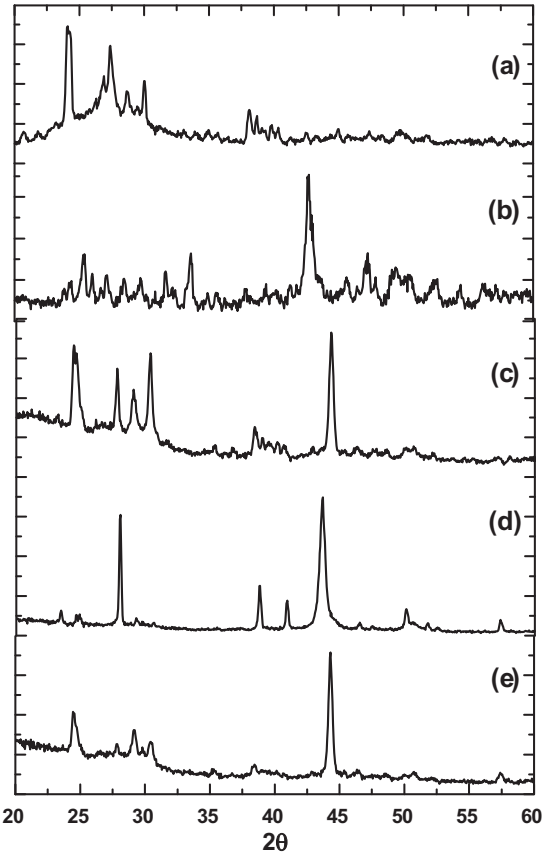

Fig. 6. XRD diagrams of (a) the synthesized $RbH(PO_3H)\cdot Te(OH)_6$ powder, (b) the tested pellet A, (c) the tested pellet B, (d) the tested pellet C and (e) the tested pellet D. The pellets A and B were tested, respectively, with platinum–carbon and gold electrodes for 135 h between 113 and 317 °C. The pellet C (earlier investigated at various temperatures up to 176 °C for 360 h) and the pellet D (heated up to 450 °C and then cooled down to room temperature prior to the measurement) were tested with gold electrodes under the same conditions as used for the pellets A and B.

investigated generally for 20–25 h at each temperature show a small decrease in the conductivity by the operating time. In contrast to the general view, the conductivity decreases remarkably by operating for 40 h at 240 °C. It can be seen that the conductivity of $RbH(PO_3H)\cdot Te(OH)_6$ depends on temperature, operating time, atmosphere and water content of flowing gases. The measured conductivity of the pellet B shows higher values than that of the pellet A and this difference in the conductivity reaches one order of magnitude at 240 °C. Fig. 9 gives two impedance spectra of both pellets A and B measured at 240 °C. The conductivities of the pellets C and D also increases by changing atmosphere from dry air to humidified air at 113 °C and by flowing gas from humidified air to humidified gas mixture of 9%H_2 in N_2 at 176 °C. The conductivity of the pellet C decreases by operating time as seen for the pellets A and B. Even though, the measured conductivity of the pellet D decreases by time under both dry and humidified air, it shows enhanced stability in the conductivity over time under humidified gas mixture of 9%H_2 in N_2.

Plots of conductivity (i.e. $\log(\sigma)$ versus $1/T$) for all pellets are given in Fig. 10. The average conductivity values are given for

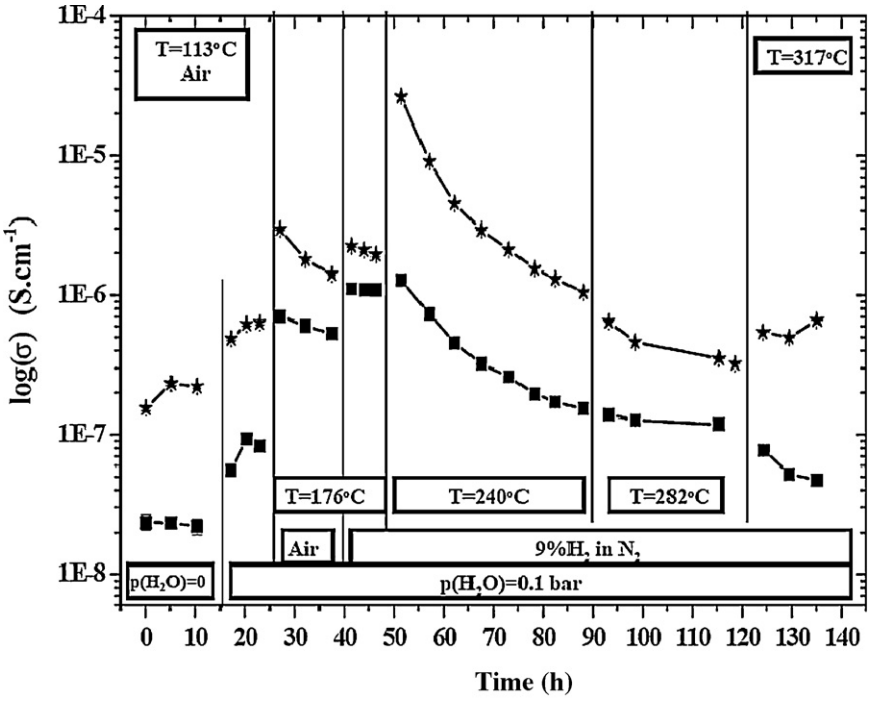

Fig. 7. Plot of conductivity (log(σ) versus time) for ■ the pellet A, * the pellet B at various temperatures and atmospheres. The pellets A and B were tested with platinum–carbon and gold electrodes, respectively.

each temperature. The conductivities of all pellets increase by increasing temperature up to 176 °C. Above that temperature the pellets B and D keep increasing in the conductivity up to 240 and 317 °C, respectively, while the pellets A and C started decreasing up to 280 °C. The conductivities of all pellets except for the pellet A shows an increase at 317 °C. The pellet C, however, shows an unexpected rise in the conductivity at that temperature.

3.3. Calculations of the equivalent capacity

Calculation of the equivalent capacity, C_ω, defined by Eq. (1) [26]:

$$C_\omega = R^{(1-\gamma)/\gamma} Q^{1/\gamma} \tag{1}$$

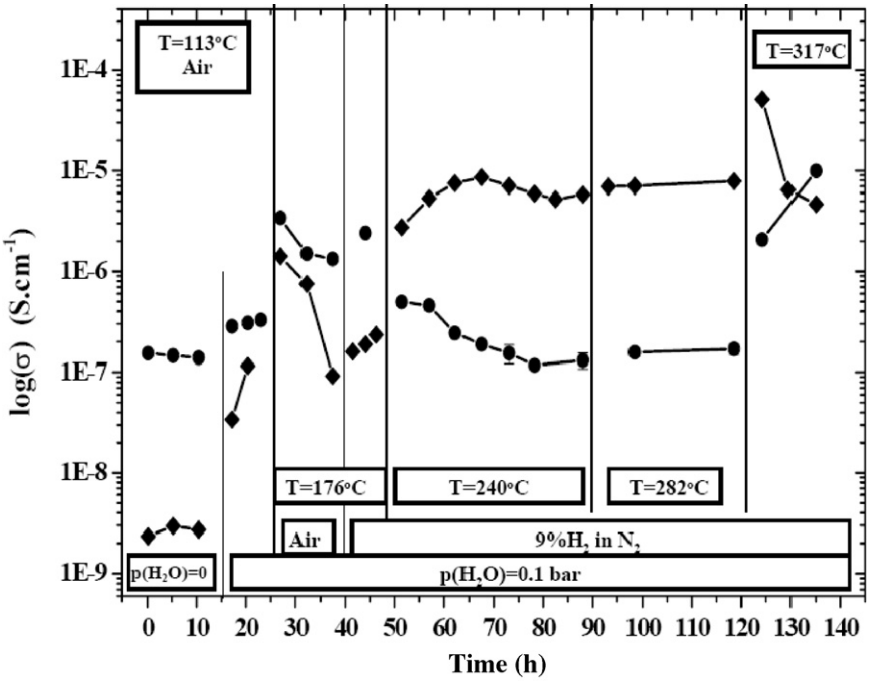

Fig. 8. Plot of conductivity (log(σ) versus time) for ● the pellet C, ◆ the pellet D at various temperatures and atmospheres. Both pellets were tested with gold electrodes.

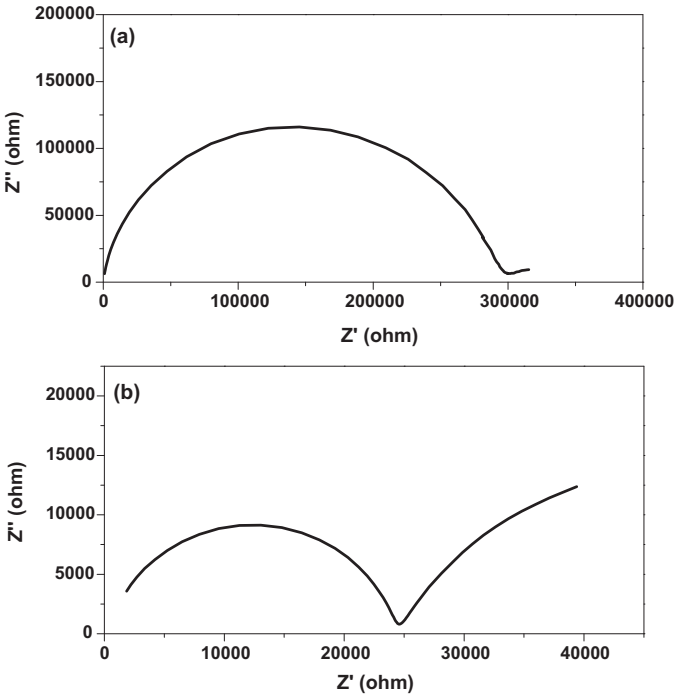

Fig. 9. Impedance spectra of (a) the pellet A and (b) the pellet B at 240 °C; the pellets A and B were tested with platinum–carbon and gold electrodes, respectively.

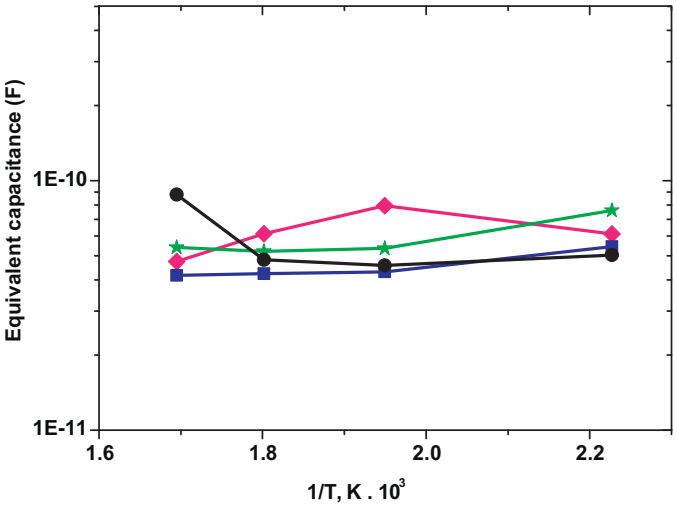

Fig. 11. Plot of equivalent capacitances versus 1/*T* for (■) the pellet A, (★) the pellet B, (●) the pellet C and (◆) the pellet D. The average equivalent capacitance values are given for each temperature. The pellets A and B were tested, respectively, with platinum–carbon and gold electrodes for 135 h between 113 and 317 °C. The pellet C (earlier investigated at various temperatures up to 176 °C for 360 h) and the pellet D (heated up to 450 °C and then cooled down to room temperature prior to the measurement) were tested with gold electrodes under the same conditions as used for the pellets A and B.

where *R* is the electrolyte resistance and *Q* is the constant phase element.

The average equivalent capacities were calculated for each temperature and their temperature dependence is given in Fig. 11. The equivalent capacities of the pellets A, B and C show similar behavior by increasing temperature and their capacities remains almost constant with change of temperature. The pellet C, however, shows an increase in the equivalent capacity at 317 °C. On the contrary, the equivalent capacity of the pellet D generally shows a decrease by increasing temperature.

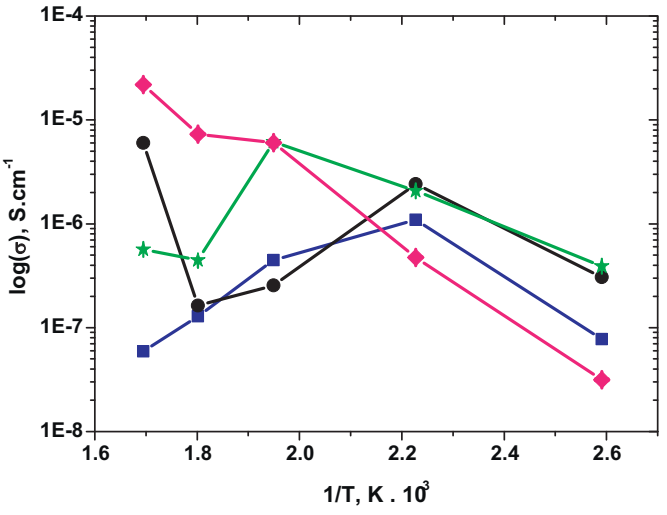

Fig. 10. Plot of conductivity (log(σ) versus 1/*T*) for (■) the pellet A, (★) the pellet B, (●) the pellet C and (◆) the pellet D. The average conductivity values are given for each temperature. The pellets A and B were tested, respectively, with platinum–carbon and gold electrodes for 135 h between 113 and 317 °C. The pellet C (earlier investigated at various temperatures up to 176 °C for 360 h) and the pellet D (heated up to 450 °C and then cooled down to room temperature prior to the measurement) were tested with gold electrodes under the same conditions as used for the pellets A and B.

4. Discussion

Referring to Fig. 3, the difference in composition (atomic %) of the synthesized $RbH(PO_3H)\cdot Te(OH)_6$ compound that is seen for each point investigated by EDS analysis may be attributed to topographical effects rather than variation of the chemical composition across the sample [27].

DTA and DSC data are in an agreement with data from conductivity measurements. It has been reported previously superprotonic phase transitions in $MH(PO_3H)$ compounds only occur for samples that exhibit a monoclinic structure [5]. Amorphous $RbH(PO_3H)\cdot Te(OH)_6$ does not show any superprotonic conductivity, this is in a good agreement with the discussion above. The results shown in Fig. 12 demonstrate that $RbH(PO_3H)\cdot Te(OH)_6$ powder does not undergo a phase transition upon heating. This observation is further confirmed by differential scanning calorimetry as given in Fig. 5.

The endothermic peak that reaches a completion at about 315 °C on the first heating cycle does not show any reverse action on the first cooling cycle. This indicates that the dehydration of $RbH(PO_3H)\cdot Te(OH)_6$ is completed at about 315 °C. This is evident not only from the DSC analysis, but also from the weight loss at 315 °C, which is in an agreement with the dimerization reaction (R2) of $RbH(PO_3H)\cdot Te(OH)_6$. The observed weight loss for $RbH(PO_3H)\cdot Te(OH)_6$ extends over a

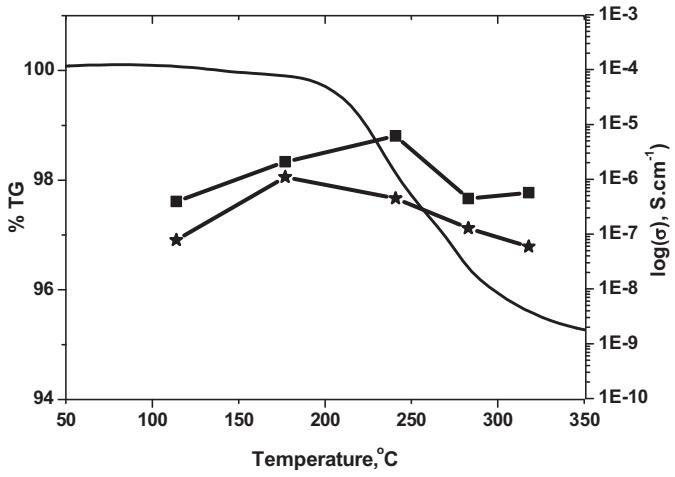

Fig. 12. Plot of conductivity log(σ) and thermal behavior TG% versus temperature for $RbH(PO_3H)\cdot Te(OH)_6$ (■ pellet A, * pellet B) The pellets A and B were tested, respectively, with platinum–carbon and gold electrodes for 135 h between 113 and 317 °C.

wide temperature ranges as reported for all phosphite salts in the literature [5].

X-ray diffraction analysis shows that synthesized $RbH(PO_3H)\cdot Te(OH)_6$ can be indexed to an amorphous and crystalline structure. All pellets were investigated up to dehydration temperature of $RbH(PO_3H)\cdot Te(OH)_6$. XRD results of the tested pellets, however, show that only pellet C reached a complete of dehydration while pellets A, B and D did not. This situation can be attributed to the difference in the operating time of the pellets. Although, the test for the pellet C was performed under the same conditions as used for the pellets A and B, it was investigated at temperatures up to 176 °C for 360 h prior to the experiment. On the other hand, pellet D was heated up to 450 °C and kept at that temperature for 2 h and then cooled down to room temperature prior to measurements. XRD results of the tested pellet D still shows both crystalline and amorphous structures. As a result of this, it can be said that $RbH(PO_3H)\cdot Te(OH)_6$ needs a heating duration of more than 2 h to be dehydrated completely at 450 °C.

All pellets show an increase in the conductivity by changing atmosphere from dry air to humidified air at 113 °C and this trend with humidified air continues between temperatures of 113–176 °C. Even though the conductivities of all pellets decrease by time at 176 °C under humidified air, yet the pellet D shows a greater decrease in the conductivity (more than one order of magnitude) as compared to others. At this temperature, all pellets also show an increase in the conductivity by changing from humidified air to humidified gas mixture of 9%H_2 in N_2. Under the gas mixture, the conductivities of all pellets decrease by time at 240 °C with the exception of the pellet D. While the pellet A tested with platinum–carbon paper electrodes shows a conductivity of 1.28×10^{-6} S cm^{-1} at 240 °C, the pellet B tested with gold electrodes reaches a conductivity value of 2.66×10^{-6} S cm^{-1} at the same temperature. This difference can be attributed to the electrode contribution, as the ohmic resistance associated with the pellet A has not been subtracted.

Moreover, the conductivities of the pellets A and B decrease to 4.04×10^{-8} S cm^{-1} and 6.6×10^{-7} S cm^{-1} at 317 °C, respectively, while pellet C, which completed the dehydration at that temperature, shows an unexpected rise in the conductivity with a value of 9.89×10^{-6} S cm^{-1}. The conductivities of the pellets A, B and C decrease during the dehydration and this behavior is in an agreement with the literature. The conductivity of the pellet C, however, starts to increase after the completion of the dehydration at 317 °C. The dehydration mechanism (see (R1)) can be responsible for this unexpected rise in the conductivity in two ways:

(1) Monoprotic $RbH(PO_3H)$ part of $RbH(PO_3H)\cdot Te(OH)_6$ compound becomes diprotic $Rb_2H_2P_2O_5$ part of $Rb_2H_2P_2O_5\cdot[Te(OH)_6]_2$ compound upon dehydration.
(2) Dehydrated compound, $Rb_2H_2P_2O_5\cdot[Te(OH)_6]_2$, has a higher hydrogen density than $RbH(PO_3H)\cdot Te(OH)_6$.

The heat treatment was done in order to investigate in depth the conductivity of dehydrated compound. In contrast to the other samples, that of applied to the pellet D shows stability under reducing atmosphere (9%H_2 in N_2). The conductivity of the pellet D reaches the value of 8.58×10^{-6} S cm^{-1} at 240 °C and remains almost constant at this value up to 317 °C. The conductivity of the pellet D shows a value of 5.41×10^{-5} S cm^{-1} at 317 °C and then it starts to decrease as a function of operating time. This behavior may be attributed to the pretreatment process for the pellet D is not long enough to dehydrate $RbH(PO_3H)\cdot Te(OH)_6$ compound totally.

Similar equivalent capacitances were calculated for the pellets A, B and C. The pellet C, however, shows an increase in the equivalent capacity at 317 °C upon the completion of the dehydration. The pellet D, which is not completely dehydrated after a 2-h heat treatment at 450 °C, shows a different behavior upon changes in temperature as compared to the other pellets.

5. Conclusions

The $RbH(PO_3H)\cdot Te(OH)_6$ compound forms in an amorphous and crystalline structure. Unlike monoclinic phosphites, super protonic conductivity is not seen in this rubidium phosphite tellurate compound. The conductivity of the compound decreases during dehydration, as expected, and average conductivity values of 5.91×10^{-8} and 5.67×10^{-7} S cm^{-1} are obtained for the pellets A and B at 317 °C, respectively. It shows that the electrode contribution, as the ohmic resistance associated with the pellet A has not been subtracted.

The pellet C shows a jump in the conductivity at 317 °C (from 2.09×10^{-6} S cm^{-1} to 9.9×10^{-6} S cm^{-1}). Although all pellets were treated under the same conditions, the pellet C was investigated up to 176 °C for 360 h prior to the experimentation. Due to the effect of operating time on dehydration, a new compound, $Rb_2H_2P_2O_5\cdot[Te(OH)_6]_2$, occurs by the dehydration of the pellet C at 317 °C. The conductivity of the pellet C reaches 9.9×10^{-6} S cm^{-1} at that temperature. Dehydration is not usually responsible for increasing conductivity. This increase in the conductivity is due to the fact that

the monoprotic $RbH(PO_3H)$ part of $RbH(PO_3H)\cdot Te(OH)_6$ becomes a diprotic $Rb_2H_2P_2O_5$ part of $Rb_2H_2P_2O_5\cdot[Te(OH)_6]_2$ compound by dehydration. The dehydrated compound has also a higher hydrogen density relative to the starting compound. For that reason, it can be assumed that the dehydration of the $RbH(PO_3H)\cdot Te(OH)_6$ enhances the conductivity. The measurements done with the pellet D, dehydrated $RbH(PO_3H)\cdot Te(OH)_6$ prior to measurement, support that the dehydrated compound have a conductivity of 5.41×10^{-5} S cm^{-1} at 317 °C. Moreover, it is seen that a dehydrated compound shows stability against operating time and temperature changes up to 317 °C. The decrease in conductivity of the pellet D at 317 °C may be attributed to the fact that the pretreatment process for the pellet D is not long enough to reach the complete dehydration.

Acknowledgements

The authors would like to thank Prof. Dr. Selahattin Gültekin of Istanbul Aydin University for scientific contributions and colleagues at Fuel Cell and Solid State Chemistry Division at Risø DTU for their assistance and discussions, especially Mogens Mogensen, Nikolaos Bonanos, Peter Holtappels and Jens F.S. Borchsenius. The Catalysis for Sustainable Energy initiative is funded by the Danish Ministry of Science, Technology and Innovation.

References

[1] S.M. Haile, C.R.I. Chisholm, K. Sasaki, D.A. Boysen, T. Uda, Solid acid proton conductors: from laboratory curiosities to fuel cell electrolytes, Faraday Discussions 134 (2007) 17–39.

[2] E.V. Kosterina, S.I. Troyanov, E. Kemnitz, L.A. Aslanov, Synthesis and crystal structure of acid phosphites RbH_2PO_3, CsH_2PO_3, and TlH_2PO_3, Russian Journal of Coordination Chemistry 27-7 (2001) 458–462.

[3] E.V. Kosterina, S.I. Troyanov, L.A. Aslanov, E. Kemnitz, Superacid univalent metal phosphites $(MH_2PO_3)_2\cdot H_3PO_3$ (M = Rb, Tl(I)) and $MH_2PO_3\cdot H_3PO_3$ (M = K, Cs): synthesis and structure, Russian Journal of Coordination Chemistry 27–28 (2001) 527–536.

[4] C.R.I. Chisholm, S.M. Haile, X-ray structure refinement of $CsHSO_4$ in phase II, Solid State Ionics 136–137 (2000) 229–241.

[5] A.S. Bondarenko, W. Zhou, H.J.M. Bouwmeester, Superprotonic $KH(PO_3H)$–SiO_2 composite electrolyte for intermediate temperature fuel cells, Journal of Power Sources 194 (2009) 843–846.

[6] L.A. Cowan, R.M. Morcos, N. Hatada, A. Nevrotsky, S.M. Haile, High temperature properties of $Rb_3H(SO_4)_2$ at ambient pressure: absence of a polymorphic, superprotonic transition, Solid State Ionics 179 (2008) 305–313.

[7] C.R.I. Chisholm, R.B. Merle, D.A. Boysen, S.M. Haile, Superprotonic phase transition in $CsH(PO_3H)$, Chem. Mater. 14 (2002) 3889–3893.

[8] W. Zhou, A.S. Bondarenko, B.A. Boukamp, H.J.M. Bouwmeester, Superprotonic conductivity in $MH(PO_3H)$ (M = Li^+, Na^+, K^+, Rb^+, Cs^+, NH_4^+), Solid State Ionics 179 (2008) 380–384.

[9] M. Dammak, H. Khemakhem, N. Zouari, A.W. Kolsi, T. Mhiri, Electrical properties of ferroelectric addition compound $K_2SeO_4\cdot Te(OH)_6$, Solid State Ionics 127 (2000) 125–132.

[10] L. Ktari, M. Dammak, A. Madani, T. Mhiri, A.W. Kolsi, Conductivity study of a new protonic conductor $Rb_{1.12}(NH_4)_{0.88}SO_4\cdot Te(OH)_6$, Solid State Ionics 145 (2001) 225–231.

[11] M. Dammak, H. Khemakhem, T. Mhiri, Superprotonic conduction and ferroelectricity in addition cesium sulfate tellurate $Cs_2SO_4\cdot Te(OH)_6$, Journal of Physics and Chemistry of Solids 62 (2001) 2069–2074.

[12] C. Boudaya, N. Chabchoub, H. Khemakhem, R. Von der Muhll, Ionic conduction and dielectric properties in the telluric sulfate $K_2(SO_4)\cdot Te(OH)_6$, Journal of Alloys and Compounds 352 (2003) 304–308.

[13] N. Chabchoub, H. Khemakhem, AC ionic conductivity investigations on the $CsK(SO_4)\cdot Te(OH)_6$ material, Journal of Alloys and Compounds 370 (2004) 8–17.

[14] L. Ktari, M. Dammak, A. Hadrich, A. Cousson, M. Nierlich, F. Romain, T. Mhiri, Solid state sciences structural, vibrational and dielectric properties of the new mixed solution $K_{0.84}(NH_4)_{1.16}SO_4\cdot Te(OH)_6$, Solid State Sciences 6 (2004) 1393–1401.

[15] H. Litaiem, M. Dammak, T. Mhiri, A. Cousson, Structural, conductivity and dielectric studies in $(NH_4)_2SeO_4\cdot Te(OH)_6$, Journal of Alloys and Compounds 396 (2005) 34–39.

[16] M. Dammak, L. Ktaria, A. Cousson, T. Mhiri, Structural and conductivity study of a new protonic conductor $Cs_{0.86}(NH_4)_{1.14}SO_4\cdot Te(OH)_6$, Journal of Solid State Chemistry 178 (2005) 2109–2116.

[17] N. Chabchoub, H. Khemakhem, R. Von der Muhll, Dielectric, electric and Raman studies on the $RbK(SO_4)\cdot Te(OH)_6$ material, Journal of Alloys and Compounds 386 (2005) 319–325.

[18] M. Abdelhedi, M. Dammak, A. Cousson, A.W. Kolsi, Structural and conductivity study of a new protonic conductor $Cs_{0.86}(NH_4)_{1.14}SO_4\cdot Te(OH)_6$, Journal of Alloys and Compounds 398 (2005) 55–61.

[19] M. Dammak, H. Litaiem, T. Mhiri, Structural, thermal and dielectric studies in $Na_2SeO_4\cdot Te(OH)_6\cdot H_2O$, Journal of Alloys and Compounds 416 (2006) 228–235.

[20] N. Chabchoub, J. Darriet, H. Khemakhem, Structural and conductivity studies of $CsKSO_4\cdot Te(OH)_6$ and $Rb_{1.25}K_{0.75}SO_4\cdot Te(OH)_6$ materials, Journal of Solid State Chemistry 179 (2006) 2164–2173.

[21] M. Dammak, A. Hadrich, T. Mhiri, Compounds structural, dielectric and vibrational studies in the dipotassium sulfate selenate tellurate mixed solid solution, Journal of Alloys and Compounds 428 (2007) 8–16.

[22] M. Dammak, H. Litaiem, P. Gravereau, T. Mhiri, A.W. Kolsi, X-ray and electrical conductivity studies in the rubidium selenate tellurate, Journal of Alloys and Compounds 442 (2007) 316–319.

[23] M. Abdelhedi, L. Ktari, M. Dammak, A. Cousson, A.W. Kolsi, DSC, structural single crystal and X-ray powder diffraction study of the ammonium sulfate selenate tellurate mixed solid solution, Journal of Alloys and Compounds 460 (2008) 147–151.

[24] L. Ktari, M. Dammak, A.W. Kolsi, A. Cousson, Neutron structural, X-ray powder and vibrational studies of the mixed solid solution rubidium ammonium sulfate tellurate, Journal of Alloys and Compounds 476 (2009) 54–59.

[25] L. Ktari, M. Abdelhedi, N. Bouhlel, M. Dammak, A. Cousson, Synthesis, calorimetric, structural and conductivity studies in a new thallium selenate tellurate adduct compound, Materials Research Bulletin 44 (2009) 1792–1796.

[26] F.W. Poulsen, N. Bonanos, S. Linderoth, M. Mogensen, B. Zachau-Christiansen, High temperature electrochemistry: ceramics and metals, in: 17th Risø International Symposium on Materials Science, Risø National Laboratory, Roskilde, Denmark, 1996.

[27] P.J. Goodhew, J. Humphreys, R. Beanland, Electron Microscopy and Analysis, 3rd ed., Taylor & Francis, 2001, , ISBN: 0 7484 0968 8.